PTEP

Prog. Theor. Exp. Phys. **2020**, 103B03 (16 pages)
DOI: 10.1093/ptep/ptaa128

On the emergence of an expanding universe from a Lorentzian matrix model

F. R. Klinkhamer*

Institute for Theoretical Physics, Karlsruhe Institute of Technology (KIT), 76128 Karlsruhe, Germany
*E-mail: frans.klinkhamer@kit.edu

Received July 8, 2020; Revised August 12, 2020; Accepted August 17, 2020; Published October 24, 2020

We present evidence that recent numerical results from the reduced classical equations of the Lorentzian IIB matrix model can be interpreted as corresponding to the emergence of an expanding universe. In addition, we propose an effective metric to describe the emerging (3+1)D spacetime. This metric gives, at all times, finite values for the Ricci and Kretschmann curvature scalars. With these results, we are able to give a heuristic discussion of the origin of the Universe in the context of the IIB matrix model.

Subject Index B25, B83

1. Introduction

The Ishibashi–Kawai–Kitazawa–Tsuchiya (IKKT) large-N matrix model [1] has been proposed as a nonperturbative definition of (9+1)D type-IIB superstring theory. The model is also known as the IIB matrix model and further discussion appears in Ref. [2].

Numerical investigations [3,4] of the Lorentzian version of the IKKT matrix model have found indications that three spatial dimensions emerge which behave differently from the remaining six spatial dimensions and that the "late-time" behavior of these three spatial dimensions may be controlled by a classical configuration of the matrices. Recently, further numerical results have been presented [5] from the matrix-model classical equations with a particular *Ansatz* for the ten bosonic matrices, where the *Ansatz* implements the split of a (3+1)D "spacetime" and a 6D "internal space."

The goal here is to present a simple check that Figs. 3–5 in Ref. [5] indeed correspond to a flat 3-space expanding with cosmic time $|t|$. In addition, we suggest an effective metric for the emerging (3+1)D spacetime and give a heuristic discussion of the origin of the Universe, assuming that the matrix model describes a new phase replacing the big bang singularity [6–8]. We have also obtained certain exact solutions of the reduced classical equations of the Lorentzian matrix model, which are presented and discussed in Appendix A. Incidentally, the adjective "classical" is to be used with caution, as will be explained in Sect. 6.

2. Procedure

The basic idea is to calculate certain observables from a simple model describing random points inside a box embedded in Euclidean 3-space and to compare them with the observables obtained from the reduced classical equations of the Lorentzian matrix model [5]. The procedure consists of six steps:

(1) Consider a cube of volume $(2\,L)^3$ in $\mathbb{R}^3$ with a constant flat metric $g_{ij}(x) = \delta_{ij}$ for spatial indices $i, j \in \{1, 2, 3\}$.

(2) Generate n points in the cube with random (uniform-distribution) values for the Cartesian coordinates x^i in the range $[-L, L] \subset \mathbb{R}$.
(3) Make diagonal $n \times n$ matrices $\widehat{X}^1$, $\widehat{X}^2$, and $\widehat{X}^3$, where the matrix $\widehat{X}^1$ has the x^1 coordinates of the n random points on the diagonal and zeros elsewhere, and similarly for the matrices $\widehat{X}^2$ and $\widehat{X}^3$.
(4) Define the 3×3 matrix $\widehat{T}$ as in Eq. (3.5) of Ref. [5] and calculate its eigenvalues $\widehat{\lambda}_i$.
(5) Define the $n \times n$ matrix $\widehat{Q}$ as in Eq. (3.7) of Ref. [5] and calculate its eigenvalues $\widehat{q}_r$ for $r = 1, \ldots, n$.
(6) Define the number $\widehat{R}^2$ as in Eq. (3.8) of Ref. [5] and calculate its value.

The explicit definitions of $\widehat{T}$, $\widehat{Q}$, and $\widehat{R}^2$ are:

$$\big(\,\widehat{T}\,\big)^{ij} \equiv \frac{1}{n}\,\mathrm{tr}\big[\widehat{X}^i \cdot \widehat{X}^j\big]\,, \tag{1a}$$

$$\widehat{Q} \equiv \delta_{ij}\,\widehat{X}^i \cdot \widehat{X}^j\,, \tag{1b}$$

$$\widehat{R}^2 \equiv \frac{1}{n}\sum_{r=1}^{n} \widehat{q}_r\,, \tag{1c}$$

where the central dot on the right-hand sides of Eqs. (1a) and (1b) stands for matrix multiplication. The flat metric δ_{ij} in Eq. (1b) effectively traces back to the space–space components of the coupling constants η_{KL} in the Lorentzian version of the IKKT matrix model [1,3], using the notation of Ref. [5] with (9+1)D indices K and L running over $\{0, 1, 2, 3, \ldots, 9\}$.

The observables obtained from the random-point model carry a hat, in order to distinguish them from the observables obtained from the classical equations of the matrix model [5].

3. Numerical results

The dimensionless length scale L of the box used in the procedure of Sect. 2 can be considered to be a function of the absolute value of the dimensionless cosmic time t:

$$L = L\big(|t|\big)\,. \tag{2}$$

The n random points from Sect. 2 are then generated inside a cube of volume

$$V_{\text{cube}}(t) = \big[2\,L(|t|)\big] \times \big[2\,L(|t|)\big] \times \big[2\,L(|t|)\big]\,. \tag{3}$$

For the moment, t is considered to be just an arbitrary cosmic-time coordinate, but t has, in fact, been found to arise from the matrix-model calculation of Ref. [5] (see Sect. 5 below for further discussion).

We start by taking $n = 10$ random points (in order to allow for a direct comparison with the results of Ref. [5]; see below) and assume the following numerical values for the box scale $L(|t|)$:

$$L(0.02) = 0.4\,, \quad L(0.25) = 0.4\,, \quad L(0.50) = 0.5\,, \quad L(0.75) = 0.65\,, \tag{4}$$

where the actual L values are chosen to obtain the desired values for $\widehat{R}^2$. In fact, the values for $\widehat{R}^2$ obtained in a typical run are shown in the top-left panel of Fig. 1. The corresponding eigenvalues $\widehat{\lambda}_i$ are shown in the middle-left panel of Fig. 1 and the corresponding eigenvalues $\widehat{q}_r$ in the bottom-left panel of Fig. 1. Two remarks are in order. First, with the small number of points ($n = 10$),

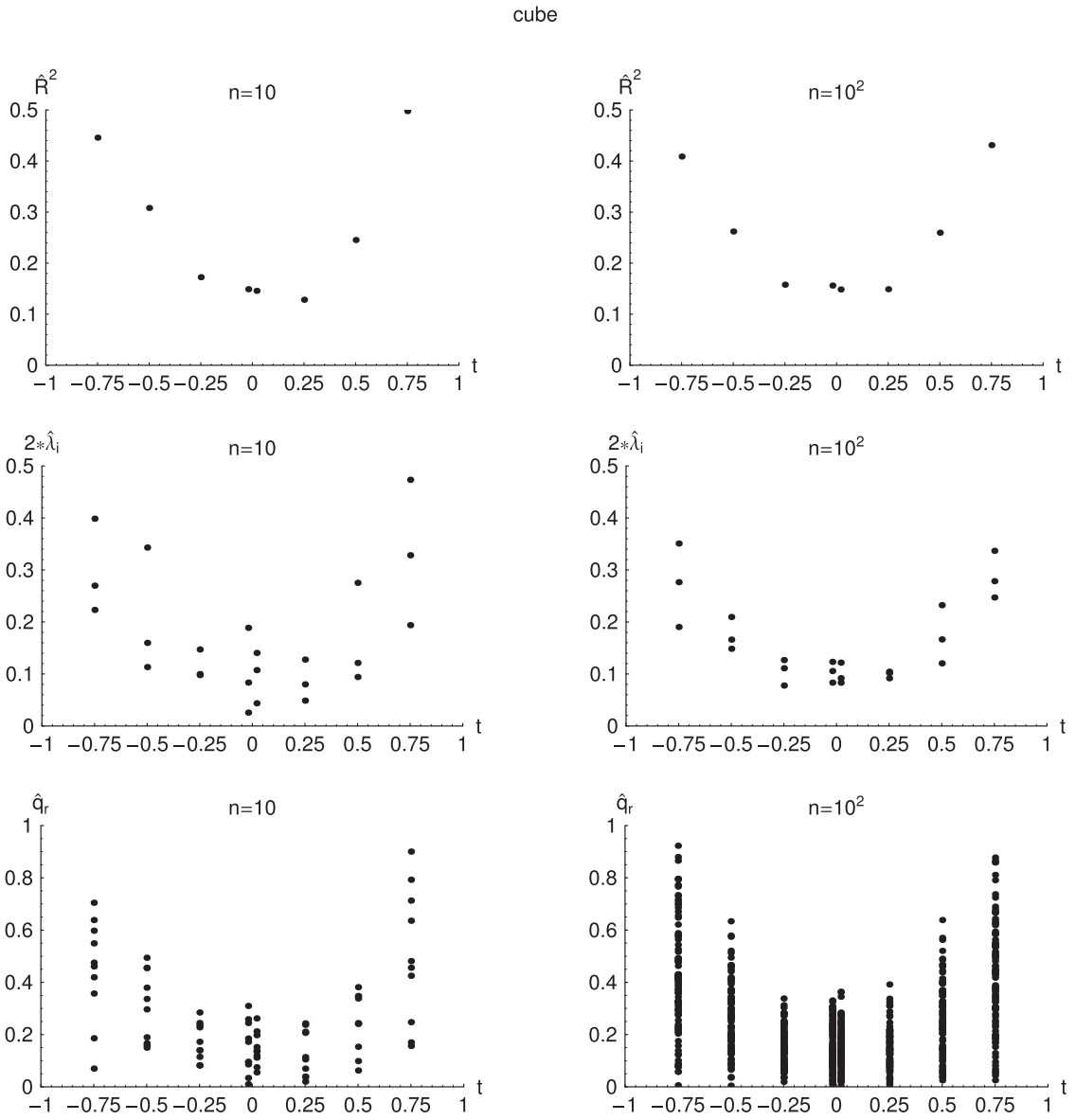

Fig. 1. Top row: Numerical results for the quantity $\widehat{R}^2$ as defined by Eq. (1c) from a typical run with a cube of volume (3) for length scales (4). The procedure used for generating the diagonal $n \times n$ matrices $\widehat{X}^i$ involves $n = 10$ (left) or $n = 10^2$ (right) random points in a cube and is outlined in Sect. 2. Middle row: Corresponding numerical results for the eigenvalues $\widehat{\lambda}_i$ of the matrix $\widehat{T}$ as defined by Eq. (1a), where actually twice the eigenvalues are plotted. Bottom row: Corresponding numerical results for the eigenvalues $\widehat{q}_r$ of the matrix $\widehat{Q}$ as defined by Eq. (1b).

the scatter of $\widehat{\lambda}_i$ values at $|t| = 0.75$ is significant. Second, in the bottom-left panel of Fig. 1, the apparently increasing gap near zero for larger and larger values of $|t|$ just appears because a larger and larger interval is covered by a fixed number (n) of points. Both issues will be discussed further below.

For a first comparison, we put $n = 10$ random points in a flattened box of volume

$$V_{\text{flattened-box}}(t) = \big[2\,L(0)\big] \times \big[2\,L(|t|)\big] \times \big[2\,L(|t|)\big], \tag{5}$$

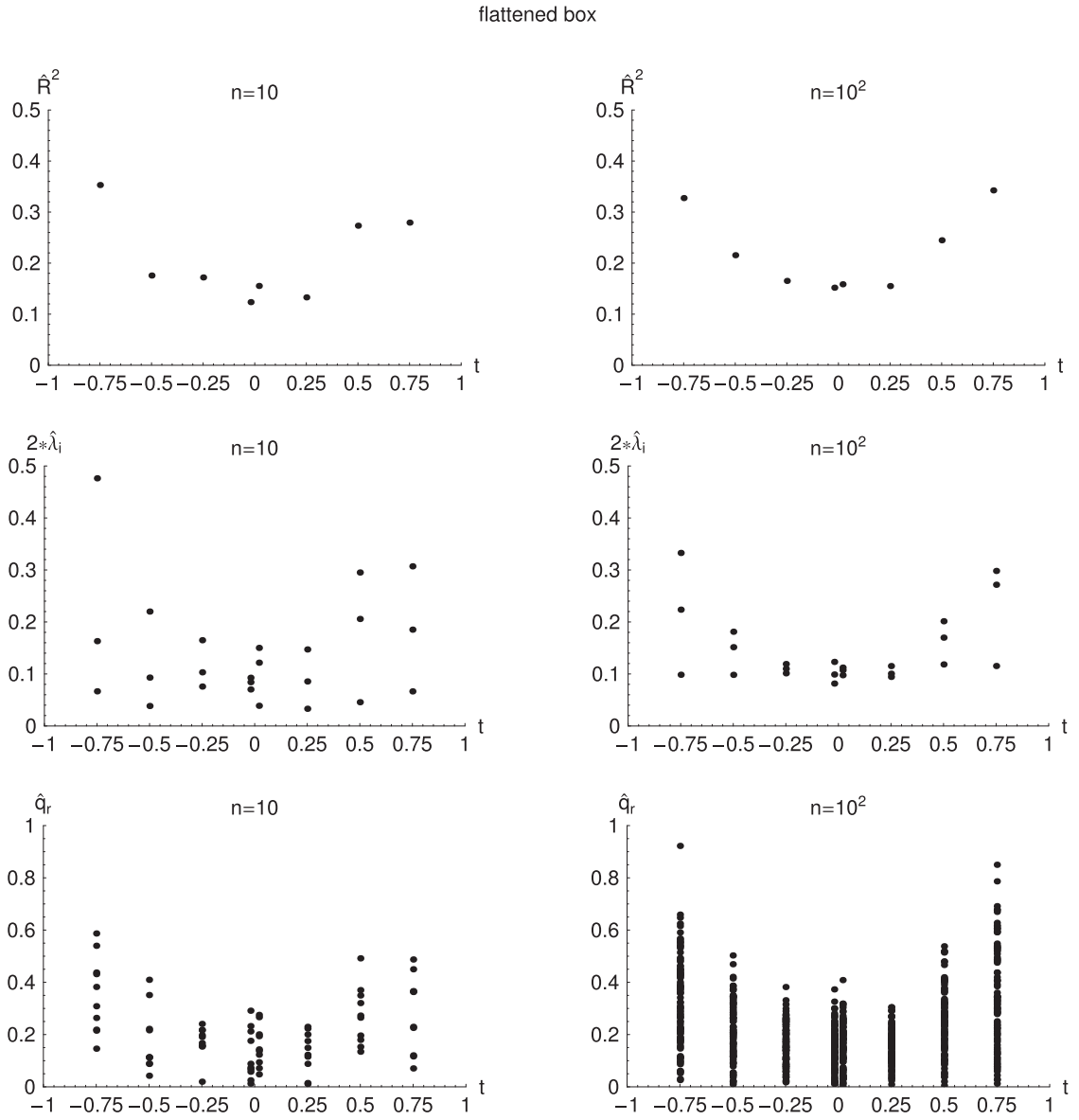

Fig. 2. Same as Fig. 1, but now for n random points in a flattened box of volume (5) for length scales (4).

with $L(0) = L(0.02)$ from Eq. (4). The corresponding numerical results are shown in the left panels of Fig. 2. The middle-left panel of Fig. 2 shows that two eigenvalues ($\widehat{\lambda}_{1,2}$) grow as $|t|$ increases, whereas one eigenvalue ($\widehat{\lambda}_3$) remains more or less constant. The behavior in the middle-left panel of Fig. 2 is fundamentally different from that in the middle-left panel of Fig. 1.

For a second comparison, we put $n = 10$ random points in a ball of radius $\widetilde{L}(t) = (6/\pi)^{1/3}\, L(t)$ and volume

$$V_{\text{ball}}(t) = (4\pi/3)\left[\widetilde{L}(t)\right]^3 = 8\left[L(t)\right]^3. \tag{6}$$

The corresponding numerical results are shown in the left panels of Fig. 3, which are qualitatively the same as those in the left panels of Fig. 1 (but there are differences, as will become clear later on).

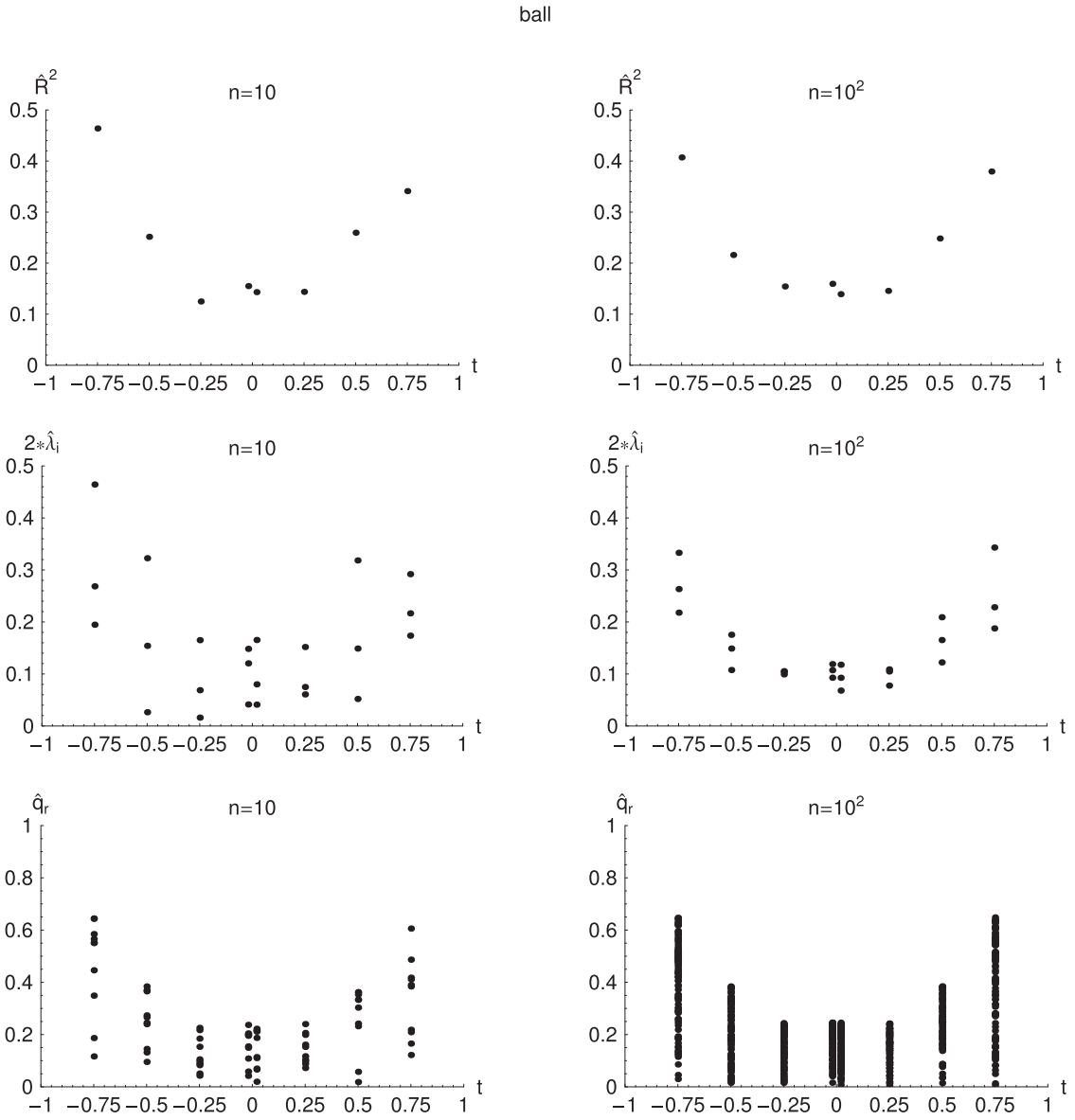

Fig. 3. Same as Fig. 1, but now for n random points in a ball of volume (6) for length scales (4).

With the simple random-point model of Sect. 2, it is easy to push the numerics further, for example, by taking $n = 10^2$ random points (the results from $n = 10^3$ random points are similar and a selection will be given later). The numerical results from $n = 10^2$ random points are given by the right panels of Figs. 1–3. The top-right and middle-right panels of Figs. 1 and 3 show a more or less stable behavior of $\widehat{R}^2(t)$ and $\widehat{\lambda}_i(t)$ (for $n \to \infty$ at fixed t, the eigenvalues $\widehat{\lambda}_i$ approach each other and $\widehat{\lambda}_i \sim \widehat{R}^2/3$), while the bottom-right panels of Figs. 1 and 3 show a dense distribution of $\widehat{q}_r$ over a range increasing with $|t|$. For $n = 10^2$ random points in the flattened box, the middle-right panel of Fig. 2 gives results similar to those for $n = 10$ in the middle-left panel, with two eigenvalues $\widehat{\lambda}_{1,2}(t)$ growing with increasing $|t|$ and a single eigenvalue $\widehat{\lambda}_3(t)$ staying more or less constant (the same behavior is seen with $n = 10^3$ random points in the flattened box).

We have already mentioned the significant spread of $\widehat{\lambda}_i$ values if the number of points is relatively small ($n = 10$) and the gaps occurring in the $\widehat{q}_r$ distribution. Figure 4 shows, for the case of a ball,

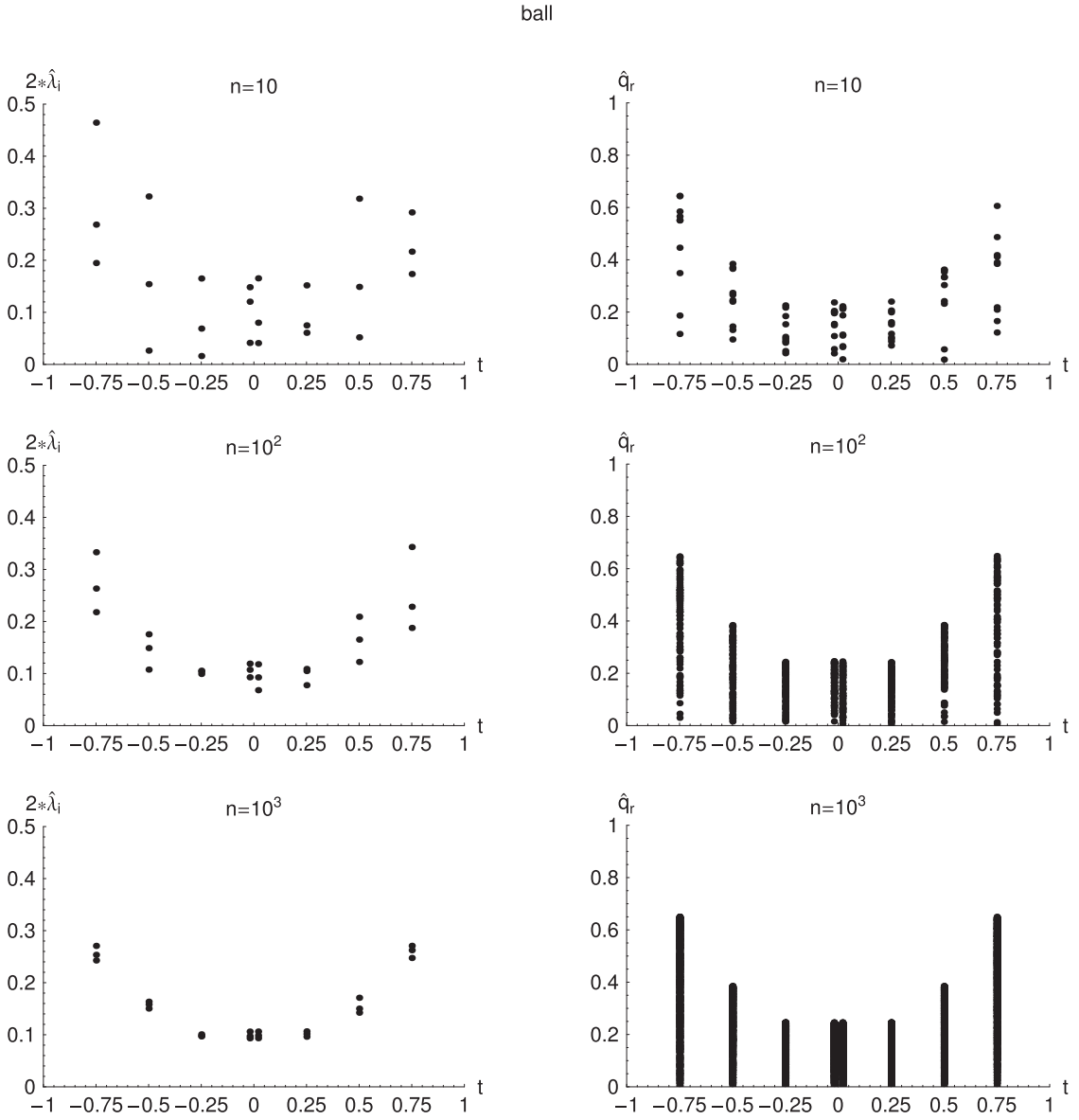

Fig. 4. Numerical results from Fig. 3, together with numerical results from $n = 10^3$ random points. The left panels show the reduction of the spread of $\widehat{\lambda}_i$ eigenvalues as n is increased, while the right panels show the augmentation of the density of $\widehat{q}_r$ eigenvalues as n is increased.

the behavior with increasing values of n. Recall that the quantity $\widehat{R}^2$ is given by the sum of the three eigenvalues $\widehat{\lambda}_i$ or, alternatively, by the average of the eigenvalues $\widehat{q}_r$, according to Eq. (1c). As to the detailed distribution of $\widehat{q}_r$ eigenvalues, Figs. 1 and 3 show some differences between the case of the cube and the case of the ball. Figure 5 gives the corresponding distributions of $\widehat{q}_r$ values for $n = 10^3$ random points and cosmic time $|t| = 0.75$.

To summarize, we have found that the left panels of Figs. 1 and 3 from the random-point-model calculations directly match Figs. 3–5 from the matrix-model calculation [5]. The conclusion is that the classical matrix-model equations (2.6) of Ref. [5] with the appropriate *Ansatz* (2.7) of Ref. [5] indeed seem to generate a cosmic time t and a flat 3-space that expands with $|t|$.

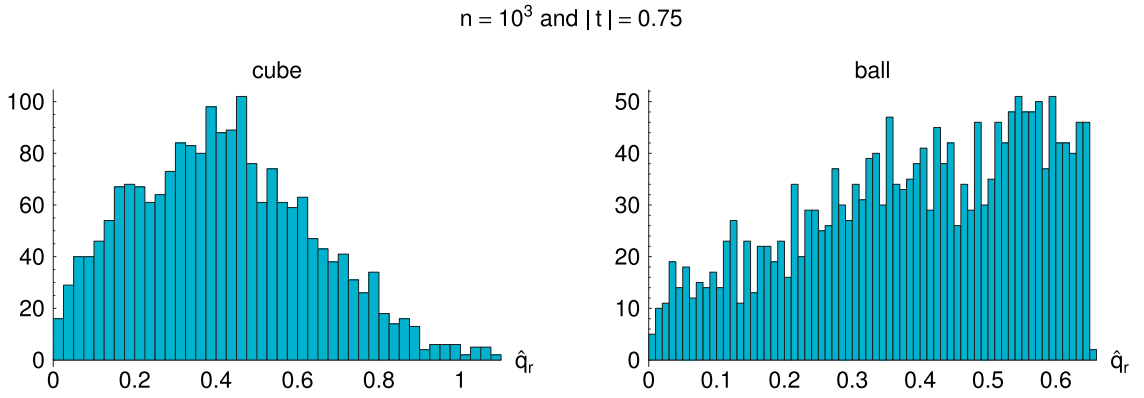

Fig. 5. Distribution of $\widehat{q}_r$ eigenvalues for the case of the cube (left) and the case of the ball (right), with $n = 10^3$ random points and at cosmic time $|t| = 0.75$.

4. Effective metric

Taking the classical results from Ref. [5] at face value and relying on the spacetime interpretation from Sect. 3, we postulate the following effective metric [6,7]:

$$ds^2\Big|^{(\text{eff})} \equiv g^{(\text{eff})}_{\mu\nu}(x)\, dx^\mu\, dx^\nu = -\frac{t^2}{t^2+b^2}\, dt^2 + a^2(t)\, \delta_{ij}\, dx^i\, dx^j\,, \tag{7a}$$

$$b > 0\,, \tag{7b}$$

$$t \in (-\infty,\, \infty)\,, \quad x^i \in (-\infty,\, \infty)\,, \tag{7c}$$

where relativistic units are used ($c = 1$) and where b can be interpreted as the length scale of a spacetime defect [9]. The individual components of $x^\mu = \left(c\,t,\, x^1,\, x^2,\, x^3\right)$ have the dimension of length.

The square of the cosmic scale factor $a(t)$ in the metric (7) can be identified with the quantity $R^2(t)$ obtained from the classical results of the large-N matrix model (see Fig. 3 of Ref. [5]). Concretely, we take

$$a(t) = L(t) \approx 0.4\left(1 + t^2/b^2\right), \tag{8}$$

which reproduces approximately the values of Eq. (4) if the dimensionless quantity t from Sect. 3 is identified with t/b here.

The actual numerical value of b in Eq. (7) is not really fixed by the matrix model (a model with only dimensionless numbers), but may perhaps be estimated [7] as $b \sim \sqrt{\alpha'}$ in terms of the Regge slope α' from the inverse string tension of the corresponding type-IIB superstring theory [1]. Here, we have switched to natural units with $\hbar = 1$ and $c = 1$.

With the effective metric (7), the Ricci curvature scalar $R(x) \equiv g^{\nu\sigma}(x)\, g^{\mu\rho}(x)\, R_{\mu\nu\rho\sigma}(x)$ and the Kretschmann curvature scalar $K(x) \equiv R^{\mu\nu\rho\sigma}(x)\, R_{\mu\nu\rho\sigma}(x)$ are given by [6]

$$R\big[a(t)\big] = \frac{6}{t^3}\left(t\left(b^2+t^2\right)\left(\frac{a'(t)}{a(t)}\right)^2 + \left[t\left(b^2+t^2\right)\frac{a''(t)}{a(t)} - b^2\,\frac{a'(t)}{a(t)}\right]\right), \tag{9a}$$

$$K\big[a(t)\big] = \frac{12}{t^6}\left(t^2\left(b^2+t^2\right)^2\left(\frac{a'(t)}{a(t)}\right)^4 + \left[t\left(b^2+t^2\right)\frac{a''(t)}{a(t)} - b^2\,\frac{a'(t)}{a(t)}\right]^2\right). \tag{9b}$$

Both curvature scalars are perfectly regular at $t = 0$ for the series $a(t) = 1+a_2\,t^2/b^2+a_4\,t^4/b^4+\cdots$; see Ref. [7] for further discussion.

Scalar metric perturbations of the background (7) have been studied in Ref. [8]. If nonrelativistic matter appears later (as argued in Sect. 6), the matter density perturbations are found to grow with $|t|$ and it is possible to define a "thermodynamic" time $\mathcal{T}(t) = |t|$. But, here, we only consider the emerging spacetime without self-gravitating perturbations.

There is, however, an important caveat. It is, namely, not at all clear that the genuine Lorentzian large-N matrix model [1–4], and not just the set of corresponding classical equations [5], also gives a nonsingular bouncing cosmology as suggested by Fig. 3 of Ref. [5] and the top-row panels of Figs. 1 and 3 here. If a cosmic bounce does not result from the matrix model, then the effective spacetime metric (7a) only holds for $t > 0$, perhaps with $b = t_{\text{emergence}} \sim \sqrt{\alpha'}$. The metric (7a) is then equivalent [6,7] to the spatially flat Robertson–Walker metric with cosmic-time coordinate $\tau \equiv \sqrt{b^2+t^2} > b = t_{\text{emergence}}$.

5. Matrix-model configurations

The authors of Ref. [5] have obtained numerical solutions of the "classical" equations for the ten bosonic $N\times N$ traceless Hermitian matrices A^K of the Lorentzian IKKT matrix model [1] (see Sect. 6 for an explanation of the quotation marks). With a particular *Ansatz* to implement the $3+6$ split of spatial dimensions found previously [3,4], the classical results of Ref. [5] indicate the emergence of a cosmic-time coordinate t and a flat 3-space expanding with $|t|$. The results of the present article support this interpretation if we compare the observables from Ref. [5] with those obtained from having random points in an expanding 3D cube or ball embedded in $\mathbb{R}^3$ (Sects. 2 and 3). In addition, we have proposed an effective metric to describe this emerging spacetime (Sect. 4).

At this point, it may be of interest to clarify the meaning of the emerging "time" in the reduced classical version of the large-N matrix model [5]. From the *Ansatz* (2.7) of Ref. [5] with $N = N_X\,N_Y$, there are four $N_X\times N_X$ Hermitian matrices X^μ, for $\mu\in\{0,\,1,\,2,\,3\}$. The particular matrix X^0, singled out by the coupling constants η_{KL}, is diagonalized and its real eigenvalues α_p, for $p\in\{1,\,2,\ldots,N_X\}$, are ordered as follows:

$$\alpha_k \leq \alpha_{k+1}\,,\quad \text{for}\quad k\in\{1,\,2,\ldots,N_X-1\}\,. \tag{10}$$

This essentially gives a dimensionless time variable t, which runs parallel to the index p of the eigenvalues α_p, as will become clear shortly.

In fact, definition (3.3) in Ref. [5] can be written as follows:

$$t_k \equiv \frac{1}{n}\sum_{r=1}^{n}\alpha_{k+r}\,, \tag{11}$$

with n a fixed number ($1\leq n < N_X$) used for averaging the eigenvalues α_p and k an index running over $\{0,\,1,\ldots,\,N_X-n\}$. In Ref. [5] and the present article, we simply write "t" for this emerging time:

$$t \equiv t_k\,. \tag{12}$$

The results of Fig. 1 in Ref. [5] show that the distance between neighboring eigenvalues α_p is more or less uniform. Write $\Delta\alpha$ for this average distance, so that $\Delta\alpha = O(1/N_X)$. Then, we have approximately

$$\alpha_p \sim \alpha_1 + (p-1)\,\Delta\alpha, \tag{13}$$

for $p \in \{1, 2, \ldots, N_X\}$. Assuming that n is even, for simplicity, definition (11) gives with Eqs. (12) and (13)

$$t \sim \alpha_{k+n/2} - \alpha_{N_X/2}\,, \tag{14}$$

where the zero of t has been defined to occur halfway, at $k = N_X/2 - n/2$. With fixed values of n and N_X, the increase of this dimensionless variable t just follows the index k on the α eigenvalues in Eq. (14).

The crucial insight, now, is that *time* is really a tool for *ordering* physical events. And the X^0 eigenvalues α_p are ordered, according to Eq. (10). Hence, the notion of time in t_k of Eq. (11) is carried by the index k, which corresponds to the index of the ordered eigenvalues from Fig. 1 in Ref. [5].

We thus have an understanding of how the cosmic time t emerges from the classical solutions of the large-N matrix model. In addition, the particular classical solutions of Ref. [5] have an emerging flat 3-space, which has been found to expand with $|t|$. The obvious question then is: *what drives this expansion?* The answer appears to be: *algebra*. How precisely the algebra produces the expansion is not yet completely clear, but we can sketch the beginning of an explanation.

The results of Fig. 2 in Ref. [5] show that the spatial matrices X^i of the classical solution are nearly diagonal, in the basis that makes X^0 perfectly diagonal (an ingredient for the definition of "t" as explained above). The effective size $R^2(t)$ of the Universe is defined by Eq. (3.4) in Ref. [5] and shown by Fig. 3 in that reference. This $R^2(t)$ behavior is more or less consistent with the behavior on the diagonal $i = j$ of Fig. 2 in Ref. [5]. Let us look at the origin of these classical solutions (or, rather, matrix-model configurations, as will be explained in Sect. 6).

The reduced classical equations are given by Eqs. (2.16) and (2.17) of Ref. [5]. For simplicity, we can take a trivial solution $Y^a = 0$ for the six internal-space $N_Y \times N_Y$ Hermitian matrices labeled by $a \in \{4, 5, \ldots, 9\}$ and having dimension $N_Y = N/N_X$. (The fermionic matrices Ψ_α, for $\alpha \in \{1, 2, \ldots, 16\}$, are also set to zero.) We then focus on the four spacetime $N_X \times N_X$ Hermitian matrices X^μ labeled by $\mu \in \{0, 1, 2, 3\}$, for which the classical "equations of motion" are [5]

$$\delta_{ij}\Big[X^i, \big[X^j, X^0\big]\Big] - \xi\, X^0 = 0\,, \tag{15a}$$

$$\eta_{\mu\nu}\Big[X^\mu, \big[X^\nu, X^i\big]\Big] - \zeta\, X^i = 0\,, \quad \text{for} \quad i \in \{1, 2, 3\}\,, \tag{15b}$$

with Lagrange multipliers $\xi \neq 0$ and $\zeta \neq 0$. We are only interested in nontrivial solutions $X^\mu \neq 0$.

Fixing the matrix size to $N_X = 64$, for definiteness, we can start with a diagonal block-type solution at $i \sim j \sim 32$ and then work out towards $i \sim j \sim 0$ and $i \sim j \sim 64$, finding that the amplitudes of the matrices X^i increase (cf. Fig. 2 in Ref. [5]). As the distance along the diagonal $i = j$ can be interpreted as the cosmic time t [roughly $t \sim (i - 32)$ for $i = 1, \ldots, 64$], we have that the X^i amplitudes grow with $|t|$, i.e., the 3-space expands (cf. Fig. 3 in Ref. [5] and the top-row panels of

Fig. 3 in the present article). Further discussion is relegated to Appendix A, which presents certain exact solutions of the reduced classical equations from the matrix model and makes a conjecture as to the algebraic origin of the expansion.

6. Discussion

Heuristically, we now have the following description of the origin of the Universe, within the context of the IIB matrix model [1,2]. The fundamental matrix model has no spacetime and no gravity, so that these physical quantities must somehow emerge from the matrices of the model.

Certain "classical" matrix solutions were presented in Ref. [5], where the quotation marks are there to alert us to the fact that the IIB matrix model has no obvious small dimensionless parameter and, therefore, no obvious saddle-point approximation. Hence, the matrices obtained are, at best, an approximation to the dominant configurations of the path integral. Still, these classical solutions (or, rather, matrix-model configurations, as they are only approximations) show a remarkable behavior that suggests an emerging spacetime having a flat 3-space expanding with time due to the algebra of the reduced equations of motion (15).

As mentioned above, gravitation and matter are expected to appear dynamically. For example, with ponderable matter present, the gravitational force will be mediated by the appropriate massless modes (virtual gravitons) of the emerging superstrings. An interesting phenomenon will be the crossover from matrix-model expansion driven by the algebra to Friedmann-type expansion driven by gravity and matter. The latter type of expansion is, strictly speaking, also due to (complicated) algebra, but that expansion can be described by Einstein's general relativity as an effective theory. It is possible that the emergent spacetime metric has the form of that of the regularized big bang singularity [6,7], which is a degenerate metric that solves the Einstein gravitational field equation and has an external length parameter (now to be determined by the matrix model).

However, at this moment, the urgent task is to show unequivocally that the matrix model [1] gives rise to the type of matrix-model configurations found in Ref. [5] and discussed in the present article.

Note added

The preprint version [10] of the present article contained an Appendix B entitled "IIB matrix model: Conceptual question", which discussed the possible role of the large-N master field for the emergence of a classical spacetime. This appendix has, however, been removed in the published version, as the content of the appendix was somewhat disconnected from the rest of the article. Three follow-up articles on the role of the IIB-matrix-model master field for the emergent classical spacetime have appeared subsequently [11–13].

Acknowledgements

We thank J. Nishimura for useful comments and acknowledge support by the KIT-Publication Fund of the Karlsruhe Institute of Technology.

Appendix A. Exact solutions of reduced equations

A.1. General solutions

In this appendix, we present certain exact solutions of the reduced classical equations from Ref. [5], in order to get a better understanding of the numerical solutions obtained in that reference. We first discuss the general solutions.

Specifically, we consider the reduced classical equations (15) for the four $N_X \times N_X$ Hermitian matrices X^μ with the following values of the Lagrange multipliers:

$$\xi = \zeta = 1\,, \tag{A.1}$$

so that the set of four equations reads explicitly

$$\sum_{j=1}^{3} \Big[X^j, \big[X^j, X^0\big]\Big] - X^0 = 0\,, \tag{A.2a}$$

$$\sum_{j\neq i} \Big[X^j, \big[X^j, X^i\big]\Big] - \Big[X^0, \big[X^0, X^i\big]\Big] - X^i = 0\,, \quad \text{for} \quad i \in \{1, 2, 3\}\,. \tag{A.2b}$$

This set of algebraic equations is surprisingly subtle. We have two preliminary remarks. First, none of the matrices X^μ can be proportional to the identity matrix (excluding the null matrix), as the commutator terms in Eq. (A.2) then vanish but the single-matrix terms do not. Second, the equations are nonlinear and allow only for a trivial sign rescaling, $X^\mu \to s^\mu\, X^\mu$, without summing over μ and with $s^\mu = (\pm 1, \pm 1, \pm 1, \pm 1)$.

We start by considering 2×2 real symmetric matrices $\widetilde{X}^\mu$, which will later be inserted on the diagonals of the respective X^μ matrices. An exact solution of the reduced classical equations (A.2), restricted to 2×2 traceless matrices, is given by:

$$\widetilde{X}^0 = \begin{pmatrix} \bar{a}_0 & 0 \\ 0 & -\bar{a}_0 \end{pmatrix}, \quad \widetilde{X}^2 = \begin{pmatrix} \bar{a}_2 & \bar{b}_2 \\ \bar{b}_2 & -\bar{a}_2 \end{pmatrix}, \tag{A.3a}$$

$$\widetilde{X}^1 = \begin{pmatrix} a_1 & b_1 \\ b_1 & -a_1 \end{pmatrix}, \quad \widetilde{X}^3 = \begin{pmatrix} a_3 & b_3 \\ b_3 & -a_3 \end{pmatrix}, \tag{A.3b}$$

with

$$\bar{a}_0 = \frac{1}{2}\sqrt{\frac{4\,{a_1}^2\,\big(1 - 4\,{b_3}^2\big) + 4\,{a_3}^2\,\big(1 - 4\,{b_1}^2\big) + 32\,a_1\,a_3\,b_1\,b_3 - 1 + 4\,{b_1}^2 + 4\,{b_3}^2}{1 - 4\,{b_1}^2 - 4\,{b_3}^2}}\,, \tag{A.3c}$$

$$\bar{a}_2 = -2\,\frac{a_1\,b_1 + a_3\,b_3}{\sqrt{1 - 4\,{b_1}^2 - 4\,{b_3}^2}}\,, \tag{A.3d}$$

$$\bar{b}_2 = \frac{1}{2}\sqrt{1 - 4\,{b_1}^2 - 4\,{b_3}^2}\,. \tag{A.3e}$$

Hence, we have a solution $\widetilde{X}^\mu$ with four moduli $\{a_1,\, b_1,\, a_3,\, b_3\}$ that lie in a particular domain D, so that the other three coefficients are real:

$$D = \Big\{(a_1,\, b_1,\, a_3,\, b_3) \in \mathbb{R}^4 \;\Big|\; \bar{a}_0 \in \mathbb{R} \,\wedge\, \bar{a}_2 \in \mathbb{R} \,\wedge\, \bar{b}_2 \in \mathbb{R}\Big\}\,. \tag{A.4}$$

We now establish that D is nonempty.

Consider a hypercube C_4 in moduli space with the center at

$$\{a_1,\, b_1,\, a_3,\, b_3\}\,\Big|^{(C_4-\text{center})} = \{1,\, 1/4,\, 1,\, 1/4\} \tag{A.5a}$$

and corners at

$$\{a_1,\, b_1,\, a_3,\, b_3\}\,\Big|^{(C_4-\text{corners})} = \{1 \pm 1/8,\, 1/4 \pm 1/16,\, 1 \pm 1/8,\, 1/4 \pm 1/16\}\,. \tag{A.5b}$$

It is then easy to verify that moduli inside this hypercube C_4 give real values for $\{\overline{a}_0,\, \overline{a}_2,\, \overline{b}_2\}$, and the conclusion is that

$$C_4 \neq \varnothing \wedge C_4 \subset D \subset \mathbb{R}^4\,. \tag{A.6}$$

Explicitly, for the moduli (A.5a) corresponding to the center of the hypercube C_4 in moduli space, we have the following solution:

$$\widetilde{X}^0 = \begin{pmatrix} \sqrt{15}/2 & 0 \\ 0 & -\sqrt{15}/2 \end{pmatrix}, \qquad \widetilde{X}^2 = \begin{pmatrix} -\sqrt{2} & 1/(2\sqrt{2}) \\ 1/(2\sqrt{2}) & \sqrt{2} \end{pmatrix}, \tag{A.7a}$$

$$\widetilde{X}^1 = \begin{pmatrix} 1 & 1/4 \\ 1/4 & -1 \end{pmatrix}, \qquad \widetilde{X}^3 = \begin{pmatrix} 1 & 1/4 \\ 1/4 & -1 \end{pmatrix}, \tag{A.7b}$$

with nonvanishing commutators $[\widetilde{X}^\mu,\, \widetilde{X}^\nu]$ for $(\mu,\, \nu) = (0,\, 1),\, (0,\, 2),\, (0,\, 3),\, (1,\, 2)$, and $(2,\, 3)$.

As to the actual shape of the manifold D from Eq. (A.4), we have three simple remarks. First, we see from the root in Eq. (A.3e) that the moduli $(b_1,\, b_3)$ lie on a disk of radius $1/(2\sqrt{2})$. Second, we see from the numerator of the root in Eq. (A.3c) that the point $(a_1,\, a_3) = (0,\, 0)$ is excluded and that $|a_1|$ and $|a_3|$ must lie above a boundary value determined by $(b_1,\, b_3)$. Third, we also see from the numerator of the root in Eq. (A.3c) that the moduli a_1 and a_3 can run off to $\pm\infty$ and we conclude that D is a noncompact manifold.

With the $\widetilde{X}^\mu$ solution (A.3) in hand, it is straightforward to construct $N_X \times N_X$ traceless Hermitian matrix solutions X^μ of the algebraic equations (A.2). Taking

$$N_X = 2\,k\,, \quad \text{for} \quad k \in \mathbb{N}_+\,, \tag{A.8a}$$

we have the following block-diagonal solutions:

$$X^\mu = \text{diag}\left(\widetilde{X}^\mu_{(1)},\, \widetilde{X}^\mu_{(2)},\, \ldots,\, \widetilde{X}^\mu_{(k)}\right)\,, \tag{A.8b}$$

where the suffixes $(1),\, (2), \ldots, (k)$ remind us that the individual blocks may have different values for the moduli, as long as these moduli remain in the domain D from Eq. (A.4).

At this moment, it may be of interest to compare our exact solutions (A.8) with the earlier exact solutions of Refs. [14,15]. Apart from one exception (mentioned in Appendix C of Ref. [16]), these earlier solutions have the property that *all* spatial matrices commute between themselves. That space–space commutativity property does not hold for the solutions presented here. For completeness, we should also mention that other space–space noncommutative solutions have been considered before; see, e.g., Ref. [16] and references therein.

A.2. Special solutions

We next investigate whether or not we can qualitatively reproduce the numerical results from Ref. [5] with the exact solutions of Appendix A.1.

In order to simplify the discussion, we take

$$N_X = 4\,l + 2\,, \quad \text{for } \; l \in \mathbb{N}_0\,. \tag{A.9}$$

There are four ingredients in our construction of a special type of solution:

(1) starting from Eq. (A.8b), assume that the moduli $\{a_1,\, b_1,\, a_3,\, b_3\}$ of the different blocks are even functions of a single dimensionless time variable τ;
(2) set $\tau = 0$ for the midway block $\widetilde{X}^{\mu}_{(l+1)}$;
(3) order the diagonal entries of X^0 by a suitable conjugation transformation (see below);
(4) perform the same conjugation transformation on the other three matrices X^i.

The conjugation transformation used in the last two ingredients traces, in fact, back to a global gauge transformation of the original matrix-model variables [1,5] and is given by

$$X^{\mu} \to \underline{X}^{\mu} = U \cdot X^{\mu} \cdot U^{\dagger}\,, \tag{A.10}$$

where U is a single unitary matrix (for us, a single orthogonal matrix). With the transformed matrices $\underline{X}^{\mu}$, we calculate the following observable [5]:

$$\Delta_{pq} \equiv \sum_{i=1}^{3} \left|\left(\underline{X}^i\right)_{pq}\right|^2\,, \tag{A.11}$$

for indices $p, q \in \{1,\, 2, \ldots, N_X\}$.

As a start, we get results for $N_X = 6$ (or $l = 1$) and explain them in detail. From the first two ingredients listed above, we have the block-diagonal solutions

$$X^{\mu} = \text{diag}\left(\widetilde{X}^{\mu}_{(\tau=-1)},\, \widetilde{X}^{\mu}_{(\tau=0)},\, \widetilde{X}^{\mu}_{(\tau=1)}\right), \tag{A.12}$$

where the 2×2 block $\widetilde{X}^{\mu}$ is given by Eq. (A.3) and τ labels the moduli of the different blocks. In fact, we take the following functions for the moduli:

$$a_1(\tau) = a_3(\tau) = 3/8 + \tau^2/4\,, \tag{A.13a}$$

$$b_1(\tau) = b_3(\tau) = 1/8\,, \tag{A.13b}$$

with $\tau \in [-1,\, 1]$. From these moduli, the three other coefficients entering the 2×2 matrices (A.3) are:

$$\overline{a}_0(\tau) = \sqrt{2/7}\,\sqrt{8\left(3/8 + \tau^2/4\right)^2 - 7/8}\,, \tag{A.14a}$$

$$\overline{a}_2(\tau) = -\sqrt{2/7}\,\left(3/8 + \tau^2/4\right), \tag{A.14b}$$

$$\overline{b}_2(\tau) = \frac{1}{4}\,\sqrt{7/2}\,. \tag{A.14c}$$

Implementing the last two ingredients listed above, the diagonal X^0 matrix from Eq. (A.12) with moduli (A.13) is reordered by use of the transformation (A.10) and the X^i matrices are transformed simultaneously. We then get the following values for the diagonal matrix $\underline{X}^0$ and the matrix Δ from Eq. (A.11):

$$\underline{X}^0 = \text{diag}\Big(-3/\sqrt{14},\; -3/\sqrt{14},\; -1/\sqrt{14},\; 1/\sqrt{14},\; 3/\sqrt{14},\; 3/\sqrt{14}\Big)\,, \tag{A.15a}$$

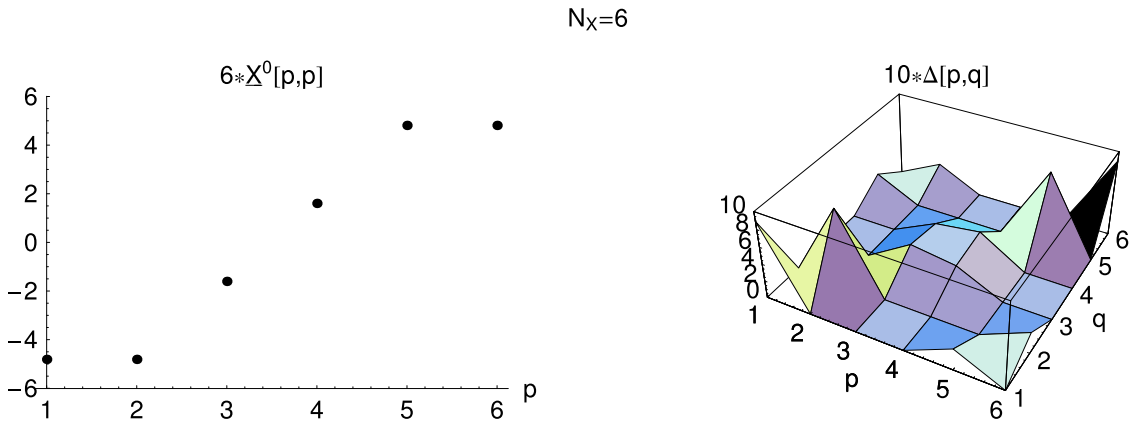

Fig. A.1. Exact solution (A.12) for $N_X = 6$ with moduli (A.13): shown are, on the left, the eigenvalues of the diagonal matrix $\underline{X}^0$ and, on the right, the matrix Δ_{pq} defined by Eq. (A.11).

$$\Delta_{pq} = \begin{pmatrix} 25/28 & 0 & 0 & 0 & 1/4 & 0 \\ 0 & 25/28 & 0 & 0 & 0 & 1/4 \\ 0 & 0 & 9/28 & 1/4 & 0 & 0 \\ 0 & 0 & 1/4 & 9/28 & 0 & 0 \\ 1/4 & 0 & 0 & 0 & 25/28 & 0 \\ 0 & 1/4 & 0 & 0 & 0 & 25/28 \end{pmatrix}_{pq}, \tag{A.15b}$$

which are also shown in Fig. A.1. The growth along the diagonal of Δ_{pq} is significant (by a factor of approximately 3, going from the middle of the diagonal towards the edges) and there is a modest jump at $\tau = 0$ in the $\underline{X}^0$ eigenvalues, but the diagonal band structure of Δ_{pq} is somewhat disturbed by small entries straddling the anti-diagonal.

It is now straightforward to generalize the $N_X = 6$ construction to larger values of N_X. With $l > 1$ defined by Eq. (A.9), the block-diagonal solutions are given by

$$X^\mu = \text{diag}\left(\widetilde{X}^\mu_{(\tau=-1)}, \ldots, \widetilde{X}^\mu_{(\tau=-2/l)}, \widetilde{X}^\mu_{(\tau=-1/l)}, \widetilde{X}^\mu_{(\tau=0)}, \widetilde{X}^\mu_{(\tau=1/l)}, \widetilde{X}^\mu_{(\tau=2/l)}, \ldots, \widetilde{X}^\mu_{(\tau=1)}\right). \tag{A.16}$$

We also make a slight change in the moduli functions (the reason for this will become clear shortly):

$$a_1(\tau) = a_3(\tau) = 1/4 + \tau^2/2\,, \tag{A.17a}$$

$$b_1(\tau) = b_3(\tau) = 1/4\,, \tag{A.17b}$$

with $\tau \in [-1, 1]$. From these moduli, the three other coefficients entering the 2×2 matrices (A.3) are:

$$\bar{a}_0(\tau) = \sqrt{\tau^2 + \tau^4}\,, \tag{A.18a}$$

$$\bar{a}_2(\tau) = -\sqrt{2}\,\left(1/4 + \tau^2/2\right), \tag{A.18b}$$

$$\bar{b}_2(\tau) = \frac{1}{2\sqrt{2}}\,, \tag{A.18c}$$

with $\bar{a}_0(0) = 0$, as desired (this is, in fact, the reason for having changed the moduli functions). Reordering the diagonal X^0 matrix from Eq. (A.16) with moduli (A.17) and transforming the X^i

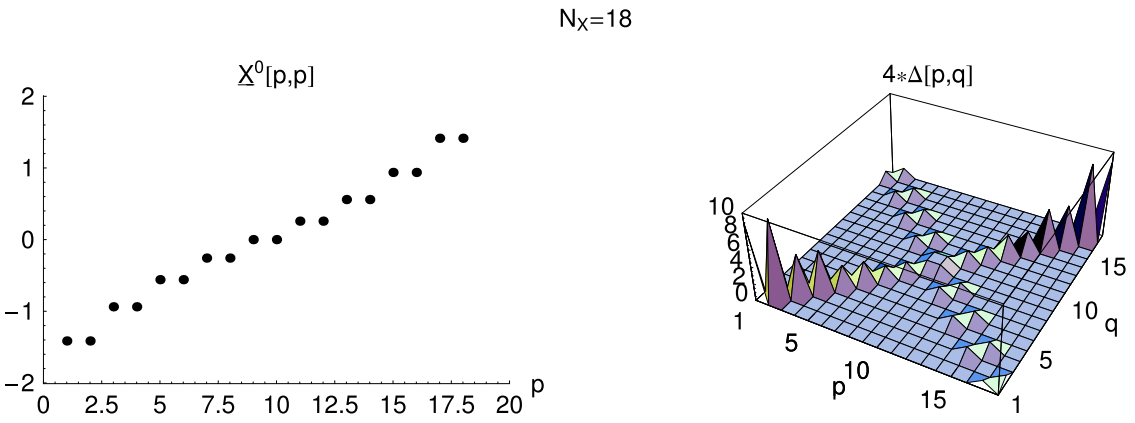

Fig. A.2. Exact solution (A.16) for $N_X = 18$ with moduli (A.17): shown are, on the left, the eigenvalues of the diagonal matrix $\underline{X}^0$ and, on the right, the matrix Δ_{pq} defined by Eq. (A.11).

simultaneously, we get the diagonal matrix $\underline{X}^0$ and the matrix Δ from Eq. (A.11). The results for $N_X = 18$ are shown in Fig. A.2. Generalization to even larger values of N_X is trivial and the results will look like those of Fig. A.2.

The exact results from Fig. A.2 are qualitatively similar to the numerical results of Figs. 1 and 2 in Ref. [5]. Admittedly, the right panel of our Fig. A.2 has some noise along the anti-diagonal, but the main feature of Δ_{pq} is the growth on the diagonal (by a factor of approximately 9, going from the middle of the diagonal towards the edges).

It still needs to be explained how the particular moduli functions (A.17) for the block-diagonal solution (A.16) come about. One conjecture is that there would be an "entropy effect" operative in the numerical procedure of Ref. [5]: the entropy for embedded block-diagonal solutions with τ-dependent moduli would be larger than the entropy for embedded block-diagonal solutions with constant (τ-independent) moduli.

References

[1] N. Ishibashi, H. Kawai, Y. Kitazawa, and A. Tsuchiya, Nucl. Phys. B **498**, 467 (1997) [arXiv:hep-th/9612115] [Search INSPIRE].
[2] H. Aoki, S. Iso, H. Kawai, Y. Kitazawa, A. Tsuchiya, and T. Tada, Prog. Theor. Phys. Suppl. **134**, 47 (1999) [arXiv:hep-th/9908038] [Search INSPIRE].
[3] S.-W. Kim, J. Nishimura, and A. Tsuchiya, Phys. Rev. Lett. **108**, 011601 (2012) [arXiv:1108.1540 [hep-th]] [Search INSPIRE].
[4] J. Nishimura and A. Tsuchiya, J. High Energy Phys. **1906**, 077 (2019) [arXiv:1904.05919 [hep-th]] [Search INSPIRE].
[5] K. Hatakeyama, A. Matsumoto, J. Nishimura, A. Tsuchiya, and A. Yosprakob, Prog. Theor. Exp. Phys. **2020**, 043B10 (2020) [arXiv:1911.08132 [hep-th]] [Search INSPIRE].
[6] F. R. Klinkhamer, Phys. Rev. D **100**, 023536 (2019) [arXiv:1903.10450 [gr-qc]] [Search INSPIRE].
[7] F. R. Klinkhamer, Phys. Rev. D **101**, 064029 (2020) [arXiv:1907.06547 [gr-qc]] [Search INSPIRE].
[8] F. R. Klinkhamer and Z. L. Wang, Phys. Rev. D **101**, 064061 (2020) [arXiv:1911.06173 [gr-qc]] [Search INSPIRE].
[9] F. R. Klinkhamer, J. Phys.: Conf. Ser. **1275**, 012012 (2019) [arXiv:1811.01078 [gr-qc]] [Search INSPIRE].
[10] F. R. Klinkhamer, arXiv:1912.12229v6 [gr-qc] [Search INSPIRE].
[11] F. R. Klinkhamer, arXiv:2007.08485 [hep-th] [Search INSPIRE].
[12] F. R. Klinkhamer, arXiv:2008.01058 [hep-th] [Search INSPIRE].
[13] F. R. Klinkhamer, [arXiv:2008.11699 [hep-th]].

[14] S.-W. Kim, J. Nishimura, and A. Tsuchiya, Phys. Rev. D **86**, 027901 (2012) [arXiv:1110.4803 [hep-th]] [Search INSPIRE].
[15] S.-W. Kim, J. Nishimura, and A. Tsuchiya, J. High Energy Phys. **1210**, 147 (2012) [arXiv:1208.0711 [hep-th]] [Search INSPIRE].
[16] H. C. Steinacker, Class. Quantum Grav. **37**, 113001 (2020) [arXiv:1911.03162 [hep-th]] [Search INSPIRE].